Neural Space-Mapping Optimization for EM-Based Design

Mohamed H. Bakr, *Student Member, IEEE*, John W. Bandler, *Fellow, IEEE*, Mostafa A. Ismail, *Student Member, IEEE*, José Ernesto Rayas-Sánchez, *Senior Member, IEEE*, and Qi-Jun Zhang, *Senior Member, IEEE*

***Abstract*—We propose, for the first time, neural space-mapping (NSM) optimization for electromagnetic-based design. NSM optimization exploits our space-mapping (SM)-based neuromodeling techniques to efficiently approximate the mapping. A novel procedure that does not require troublesome parameter extraction to predict the next point is proposed. The initial mapping is established by performing upfront fine-model analyses at a reduced number of base points. Coarse-model sensitivities are exploited to select those base points. Huber optimization is used to train, without testing points, simple SM-based neuromodels at each NSM iteration. The technique is illustrated by a high-temperature superconducting quarter-wave parallel coupled-line microstrip filter and a bandstop microstrip filter with quarter-wave resonant open stubs.**

***Index Terms*—Design automation, EM optimization, microwave circuits, microstrip filters, neural-network applications, neural space mapping, neural modeling, optimization methods, space mapping.**

I. Introduction

ARTIFICIAL neural networks (ANNs) are suitable models for microwave circuit yield optimization and statistical design [1], [2]. Neuromodels are computationally much more efficient than electromagnetic (EM) or physical models and can be more accurate than empirical physics-based models. Once they are trained with reliable learning data, obtained by either EM simulation or by measurement, the neuromodel can be used for efficient and accurate optimization within the region of training. This has been the conventional approach to optimization of microwave structures using ANNs [3].

The principal drawback of this ANN optimization approach is the cost of generating sufficient learning samples, since the simulations/measurements must be performed for many combinations of different values of geometrical, material, process, and input signal parameters over a large region. Additionally, it is well known that the extrapolation ability of neuromodels is poor, making unreliable any solution predicted outside the training region. Introducing knowledge, as in [4], can alleviate these limitations.

A powerful new method for optimization of microwave circuits based on space-mapping (SM) technology and ANNs is presented. An innovative strategy is proposed to exploit the SM-based neuromodeling techniques [5] in an efficient neural space-mapping (NSM) optimization algorithm, including frequency. NSM requires a reduced set of upfront learning base points. A "coarse" or empirical model is used not only as source of knowledge that reduces the amount of learning data and improves the generalization performance of the SM-based neuromodel, but also as a means to select the initial learning base points through sensitivity analysis. A novel procedure that does not require troublesome parameter extraction to predict the next point is presented. Huber optimization is used to train the SM-based neuromodels at each iteration. The SM-based neuromodels are developed without using testing points: their generalization performance is controlled by gradually increasing their complexity starting with a three-layer perceptron with zero hidden neurons. NSM optimization is illustrated by a high-temperature superconducting (HTS) quarter-wave parallel coupled-line microstrip filter and a bandstop microstrip filter with quarter-wave resonant open stubs.

II. SM Concept Including Frequency

SM is a powerful concept for circuit design and optimization that combines the computational efficiency of "coarse" models with the accuracy of "fine" models. The coarse models are typically equivalent-circuit models, which are computationally very efficient, but often have a limited validity range for their parameters, beyond which the simulation results may become inaccurate. On the other hand, fine models can be provided by an EM simulator, or even by direct measurements: they are very accurate, but CPU intensive. SM establishes a mathematical link between the coarse and fine models. It directs the bulk of CPU intensive evaluations to the coarse model, while preserving the accuracy and confidence offered by the fine model. The SM technique was originally developed by Bandler *et al.* [6].

In the SM technique with frequency dependence, the operating frequency ω is also included in the mapping function. This allows us to simulate the coarse model at a different frequency ω_c.

Let the vectors $\boldsymbol{x}_c$ and $\boldsymbol{x}_f$ represent the design parameters of the coarse and fine models, respectively, and $\boldsymbol{R}_c(\boldsymbol{x}_c, \omega_c)$ and

Manuscript received February 27, 2000; revised August 21, 2000. This work was supported in part by the Natural Sciences and Engineering Research Council of Canada under Grant OGP0007239 and Grant STP0201832 and under the Micronet Network of Centres of Excellence. The work of J. E. Rayas-Sánchez was supported by the Consejo Nacional de Ciencia y Tecnología and by the Instituto Tecnológico y de Estudios Superiores de Occidente. The work of M. H. Bakr was supported under an Ontario Graduate Scholarship.

M. H. Bakr, M. A. Ismail, and J. E. Rayas-Sánchez are with the Simulation Optimization Systems Research Laboratory and the Department of Electrical and Computer Engineering, McMaster University, Hamilton, ON, Canada L8S 4K1.

J. W. Bandler is with the Simulation Optimization Systems Research Laboratory and the Department of Electrical and Computer Engineering, McMaster University, Hamilton, Ontario, Canada L8S 4K1 and also with the Bandler Corporation, Dundas, ON, Canada L9H 5E7.

Q.-J. Zhang is with the Department of Electronics, Carleton University, Ottawa, ON, Canada K1S 5B6.

Publisher Item Identifier S 0018-9480(00)10724-0.

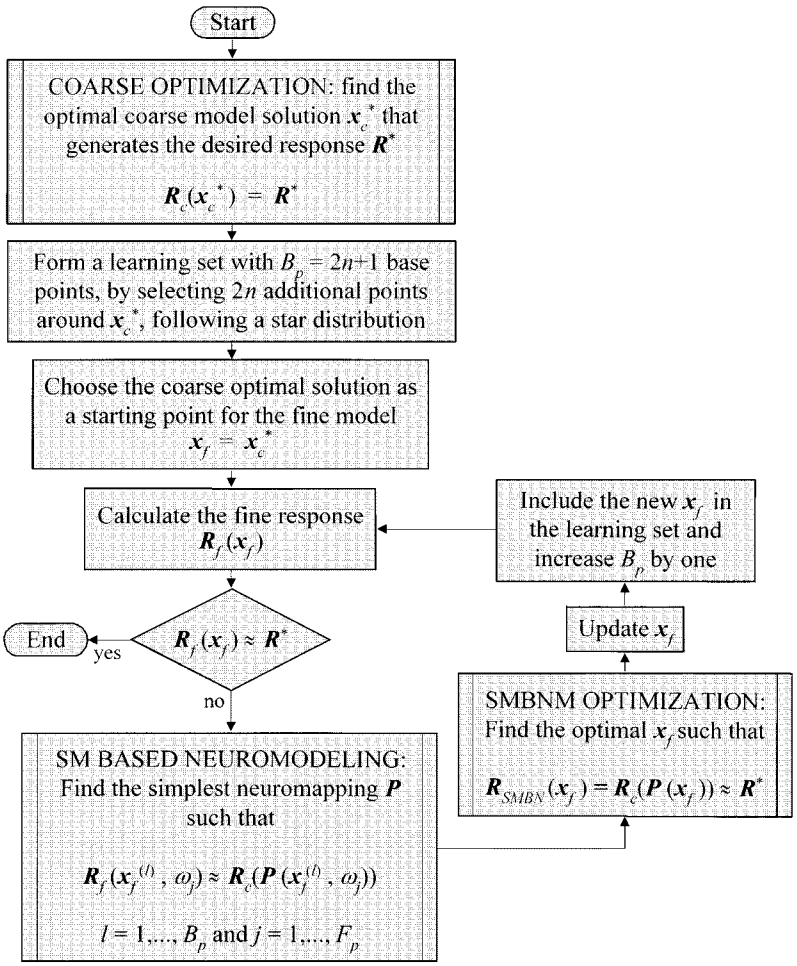

Fig. 1. NSM optimization.

$\boldsymbol{R}_f(\boldsymbol{x}_f, \omega)$ represent the corresponding model responses (e.g., $\boldsymbol{R}_c$ and $\boldsymbol{R}_f$ might contain the real and imaginary parts of S_{21}). $\boldsymbol{R}_c$ is much faster to calculate, but less accurate than $\boldsymbol{R}_f$.

The aim of SM optimization, including frequency, is to find an appropriate mapping $\boldsymbol{P}$ from the fine-model input space to the coarse-model input space

$$\begin{bmatrix} \boldsymbol{x}_c \\ \omega_c \end{bmatrix} = \boldsymbol{P}(\boldsymbol{x}_f, \omega) \tag{1}$$

such that

$$\boldsymbol{R}_c(\boldsymbol{x}_c, \omega_c) \approx \boldsymbol{R}_f(\boldsymbol{x}_f, \omega). \tag{2}$$

Once a mapping $\boldsymbol{P}$ valid in the region of interest is found, the coarse model can be used for fast and accurate simulations in that region.

III. NSM Optimization An Overview

Fig. 1 shows the flow diagram of NSM optimization. Here, we explain the overall operation of NSM optimization; a detailed description of the main blocks is presented in the following sections.

We start by finding the optimal solution $\boldsymbol{x}_c^*$ that yields the desired response using the coarse model. We select $2n$ additional points following an n-dimensional star distribution [5], [7] centered at $\boldsymbol{x}_c^*$, as shown in Fig. 2, where n is the number of design parameters ($\boldsymbol{x}_c, \boldsymbol{x}_f \in \Re^n$). The percentage of deviation from $\boldsymbol{x}_c^*$ for each design parameter is determined according to the coarse-model sensitivities. The larger the sensitivity of the coarse-model response with respect to a certain parameter, the smaller the percentage of variation of that parameter. We assume that the coarse-model sensitivities are similar to those of the fine model.

The fine-model response $\boldsymbol{R}_f$ at the optimal coarse-model solution $\boldsymbol{x}_c^*$ is then calculated. If $\boldsymbol{R}_f$ is approximately equal to the desired response, the algorithm ends, otherwise we develop an SM-based neuromodel over the $2n+1$ fine-model points.

Once an SM-based neuromodel with small learning errors is available, *we use it as an improved coarse model*, optimizing its parameters to generate the desired response. The solution to this optimization problem becomes the next point in the fine-model parameter space, and it is included in the learning set.

We calculate the fine-model response at the new point, and compare it with the desired response. If it is still different, we retrain the SM-based neuromodel over the extended set of learning samples and the algorithm continues. If not, the algorithm terminates.

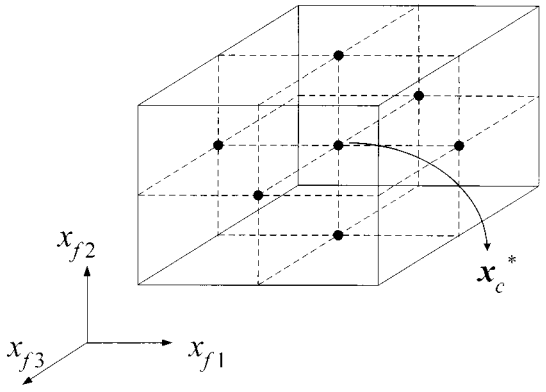

Fig. 2. Three-dimensional star distribution for the initial base points.

IV. Coarse Optimization

During the coarse optimization phase of NSM optimization, we want to find the optimal coarse-model solution $\boldsymbol{x}_c^*$ that generates the desired response over the frequency range of interest. The vector of coarse-model responses $\boldsymbol{R}_c$ might contain m different responses of the circuit

$$\boldsymbol{R}_c(\boldsymbol{x}_c) = \left[\boldsymbol{R}_c^1(\boldsymbol{x}_c)^T \ldots \boldsymbol{R}_c^m(\boldsymbol{x}_c)^T\right]^T \tag{3}$$

where each individual response has been sampled at F_p frequency points

$$\boldsymbol{R}_c^r(\boldsymbol{x}_c) = \left[R_c^r(\boldsymbol{x}_c,\omega_1)\ldots R_c^r\left(\boldsymbol{x}_c,\omega_{F_p}\right)\right]^T, \qquad r=1,\ldots,m \tag{4}$$

The desired response $\boldsymbol{R}^*$ is expressed in terms of specifications. The problem of circuit design using the coarse model can be formulated as [8]

$$\boldsymbol{x}_c^* = \arg\min_{\boldsymbol{x}_c} U\big(\boldsymbol{R}_c(\boldsymbol{x}_c)\big) \tag{5}$$

where U is a suitable objective function. For example, U could be a minimax objective function expressed in terms of upper and lower specifications for each response and frequency sample. A rich collection of objective functions, for different design constraints, is formulated by Bandler *et al.* in [8].

V. Training the SM-Based Neuromodel During NSM Optimization

At the ith iteration, we want to find the simplest neuromapping $\boldsymbol{P}^{(i)}$ such that the coarse model using that mapping approximates the fine model at all the learning points. This is realized by solving the optimization problem

$$\boldsymbol{w}^* = \arg\min_{\boldsymbol{w}} \left\| \left[\cdots \boldsymbol{e}_s^T \cdots\right]^T \right\| \tag{6}$$

with

$$\boldsymbol{e}_s = \boldsymbol{R}_f\left(\boldsymbol{x}_f^{(l)},\omega_j\right) - \boldsymbol{R}_c\left(\boldsymbol{x}_{c_j}^{(l)},\omega_{c_j}\right) \tag{7a}$$

$$\begin{bmatrix}\boldsymbol{x}_{c_j}^{(l)}\\ \omega_{c_j}\end{bmatrix} = \boldsymbol{P}^{(i)}\left(\boldsymbol{x}_f^{(l)},\omega_j,\boldsymbol{w}\right) \tag{7b}$$

$$j = 1,\ldots,F_p \tag{7c}$$

$$l = 1,\ldots,2n+i \tag{7d}$$

$$s = j + F_p(l-1) \tag{7e}$$

where $2n+i$ is the number of training base points for the input design parameters and F_p is the number of frequency points per frequency sweep. It is seen that the total number of learning samples at the ith iteration is $s=(2n+i)F_p$.

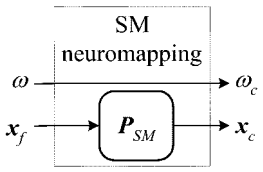

Fig. 3. Space-mapped neuromapping.

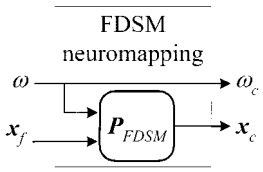

Fig. 4. Frequency-dependent space-mapped neuromapping.

Equation (7b) is the input–output relationship of the ANN that implements the mapping at the ith iteration. Vector $\boldsymbol{w}$ contains the internal parameters (weights, bias, etc.) of the ANN. The paradigm chosen to implement $\boldsymbol{P}$ is a three-layer perceptron.

All the SM-based neuromodeling techniques proposed in [5] can be exploited to efficiently solve (6). In the space-mapped neuromodeling (SMN) approach, only the design parameters are mapped, as illustrated in Fig. 3, and both models use the same frequency

$$\begin{bmatrix}\boldsymbol{x}_{c_j}^{(l)}\\ \omega_{c_j}\end{bmatrix} = \boldsymbol{P}^{(i)}\left(\boldsymbol{x}_f^{(l)},\omega_j,\boldsymbol{w}\right) = \begin{bmatrix}\boldsymbol{P}_{SM}^{(i)}\left(\boldsymbol{x}_f^{(l)},\boldsymbol{w}\right)\\ \omega_j\end{bmatrix}. \tag{8}$$

In the frequency-dependent space mapped neuromodeling (FDSMN) approach, illustrated in Fig. 4, both coarse and fine models are simulated at the same frequency, but the mapping from the fine to the coarse parameter space is dependent on the frequency

$$\begin{bmatrix}\boldsymbol{x}_{c_j}^{(l)}\\ \omega_{c_j}\end{bmatrix} = \boldsymbol{P}^{(i)}\left(\boldsymbol{x}_f^{(l)},\omega_j,\boldsymbol{w}\right) = \begin{bmatrix}\boldsymbol{P}_{FDSM}^{(i)}\left(\boldsymbol{x}_f^{(l)},\omega_j,\boldsymbol{w}\right)\\ \omega_j\end{bmatrix}. \tag{9}$$

The frequency space-mapped neuromodeling (FSMN) technique (see Fig. 5) establishes a mapping not only for the design parameters, but also for the frequency variable, such that the coarse model is simulated at a different frequency to match the fine-model response

$$\begin{bmatrix}\boldsymbol{x}_{c_j}^{(l)}\\ \omega_{c_j}\end{bmatrix} = \boldsymbol{P}^{(i)}\left(\boldsymbol{x}_f^{(l)},\omega_j,\boldsymbol{w}\right) = \left[\boldsymbol{P}_{FSM}^{(i)}\left(\boldsymbol{x}_f^{(l)},\omega_j,\boldsymbol{w}\right)\right]. \tag{10}$$

For those cases where the shapes of the fine- and coarse-model responses are nearly identical, but shifted in frequency, the frequency mapped neuromodeling technique (see Fig. 6) simulates the coarse model with the same physical parameters used by the fine model, but at a different frequency to align both responses

$$\begin{bmatrix}\boldsymbol{x}_{c_j}^{(l)}\\ \omega_{c_j}\end{bmatrix} = \boldsymbol{P}^{(i)}\left(\boldsymbol{x}_f^{(l)},\omega_j,\boldsymbol{w}\right) = \begin{bmatrix}\boldsymbol{x}_f^{(l)}\\ P_{FM}^{(i)}\left(\boldsymbol{x}_f^{(l)},\omega_j,\boldsymbol{w}\right)\end{bmatrix}. \tag{11}$$

Finally, the frequency partial-space mapped neuromodeling (FPSMN) technique maps only some of the design parameters

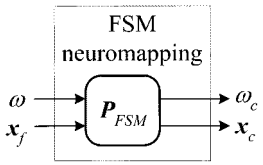

Fig. 5. Frequency space-mapped neuromapping.

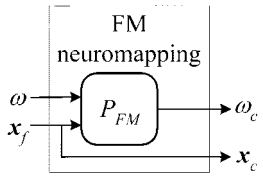

Fig. 6. Frequency-mapped neuromapping.

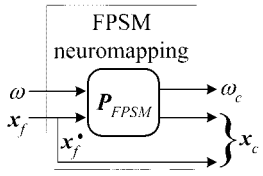

Fig. 7. Frequency partial-space mapped neuromapping.

and the frequency (see Fig. 7), making an even more efficient use of the implicit knowledge in the coarse model

$$\begin{aligned}\begin{bmatrix} \boldsymbol{x}_{c_j}^{(l)} \\ \omega_{c_j} \end{bmatrix} &= \boldsymbol{P}^{(i)}\left(\boldsymbol{x}_f^{(l)}, \omega_j, \boldsymbol{w}\right) \\ &= \begin{bmatrix} \boldsymbol{x}_f^{\bullet(l)} \\ \boldsymbol{x}_{c_j}^{\bullet(l)} \\ \omega_{c_j} \end{bmatrix} \\ &= \begin{bmatrix} \boldsymbol{x}_f^{\bullet(l)} \\ \boldsymbol{P}_{FPSM}^{(i)}\left(\boldsymbol{x}_f^{(l)}, \omega_j, \boldsymbol{w}\right) \end{bmatrix}. \end{aligned} \tag{12}$$

Note that the "design" parameters of the coarse model do not change with frequency only in the SMN and FM neuromappings.

The starting point for the first training process is a unit mapping, i.e., $\boldsymbol{P}^{(0)}(\boldsymbol{x}_f^{(l)}, \omega_j, \boldsymbol{w}_u) = [\boldsymbol{x}_f^{(l)T}\omega_j]^T$, for $j = 1, \ldots, F_p$ and $l = 1, \ldots, 2n+1$, where $\boldsymbol{w}_u$ contains the internal parameters of the ANN that give a unit mapping. The SM-based neuromodel is trained in the next iterations using the previous mapping as the starting point.

The complexity of the ANN (the number of hidden neurons and the SM-based neuromodeling technique) is gradually increased according to the learning error ε_L, starting with a linear mapping (three-layer perceptron with zero hidden neurons). In other words, we use the simplest ANN that yields an acceptable learning error ε_L, defined as

$$\varepsilon_L = \left\| \left[\cdots \boldsymbol{e}_s^T \cdots \right]^T \right\| \tag{13}$$

where $\boldsymbol{e}_s$ is obtained from (7) using the current optimal values for the ANN internal parameters $\boldsymbol{w}^*$.

In our implementation, the neuromapping for the first iteration is approximated using the FMN technique so that any possible severe misalignment in frequency between the coarse- and fine-model responses is first alleviated. The physical parameters are then gradually mapped, following an FPSMN technique.

Linear adaptive frequency-space mapping (LAFSM) is a special case of NSM optimization, corresponding to the situation when the number of hidden neurons of the ANN is zero at all iterations.

VI. SM-Based Neuromodel Optimization

At the ith iteration of NSM optimization, we use an SM-based neuromodel with small learning error as an improved coarse model, optimizing its parameters to generate the desired response. We denote the SM-based neuromodel response as $\boldsymbol{R}_{SMBN}$, defined as

$$\boldsymbol{R}_{SMBN}(\boldsymbol{x}_f) = \left[\boldsymbol{R}_{SMBN}^1(\boldsymbol{x}_f)^T \ldots \boldsymbol{R}_{SMBN}^m(\boldsymbol{x}_f)^T \right]^T \tag{14}$$

where

$$\begin{aligned}\boldsymbol{R}_{SMBN}^r(\boldsymbol{x}_f) = \left[R_c^r(\boldsymbol{x}_{c1}, \omega_{c1}) \ldots R_c^r\left(\boldsymbol{x}_{cF_p}, \omega_{cF_p}\right) \right]^T, \\ r = 1, \ldots, m \end{aligned} \tag{15}$$

with

$$\begin{bmatrix} \boldsymbol{x}_{c_j} \\ \omega_{c_j} \end{bmatrix} = \boldsymbol{P}^{(i)}(\boldsymbol{x}_f, \omega_j, \boldsymbol{w}^*) \tag{16}$$

$$j = 1, \ldots, F_p. \tag{17}$$

The solution to the following optimization problem becomes the next iterate:

$$\boldsymbol{x}_f^{(2n+i+1)} = \arg\min_{\boldsymbol{x}_f} U\left(\boldsymbol{R}_{SMBN}(\boldsymbol{x}_f)\right) \tag{18}$$

with U defined as in (5). If an SM neuromapping is used to implement $\boldsymbol{P}^{(i)}$ (see Fig. 3), the next iterate can be obtained in a simpler manner by solving

$$\boldsymbol{x}_f^{(2n+i+1)} = \arg\min_{\boldsymbol{x}_f} \left\| \boldsymbol{P}_{SM}^{(i)}(\boldsymbol{x}_f, \boldsymbol{w}^*) - \boldsymbol{x}_c^* \right\|. \tag{19}$$

VII. NSM Algorithm

Step 0) Find $\boldsymbol{x}_c^*$ by solving (5).

Step 1) Choose $\boldsymbol{x}_f^{(1)}, \ldots, \boldsymbol{x}_f^{(2n)}$ following a star distribution around $\boldsymbol{x}_c^*$.

Step 2) Initialize $i = 1, \boldsymbol{x}_f^{(2n+i)} = \boldsymbol{x}_c^*$.

Step 3) Stop if $\|\boldsymbol{R}_f(\boldsymbol{x}_f^{(2n+i)}, \omega_j) - \boldsymbol{R}_c(\boldsymbol{x}_c^*, \omega_j)\| \leq \varepsilon_R, j = 1, \ldots, F_p$.

Step 4) Initialize $\boldsymbol{P}^{(i)} = \boldsymbol{P}^{(i-1)}$, where

$$\begin{aligned}\boldsymbol{P}^{(0)}\left(\boldsymbol{x}_f^{(l)}, \omega_j, \boldsymbol{w}_u\right) = \begin{bmatrix} \boldsymbol{x}_f^{(l)} \\ \omega_j \end{bmatrix}, \\ j = 1, \ldots, F_p; \quad l = 1, \ldots, 2n+i. \end{aligned}$$

Step 5) Find $\boldsymbol{w}^*$ by solving (6).

Step 6) Calculate ε_L using (13).

Step 7) If $\varepsilon_L > \varepsilon_{\min}$, increase the complexity of $\boldsymbol{P}^{(i)}$ and go to Step 5.

Step 8) If an SM neuromapping is used to implement $\boldsymbol{P}^{(i)}$, solve (19), otherwise solve (18).

Step 9) Set $i = i + 1$; go to Step 3.

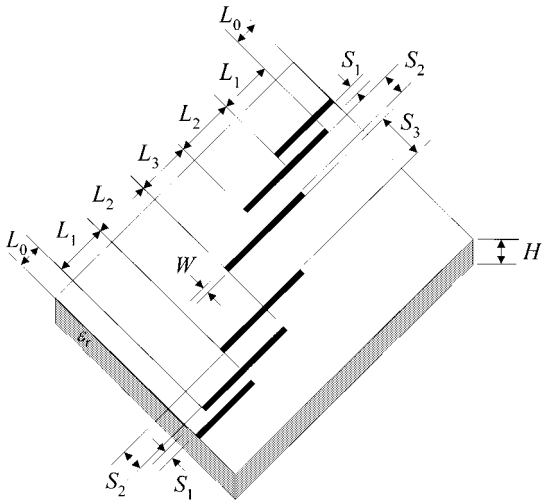

Fig. 8. HTS quarter-wave parallel coupled-line microstrip filter.

VIII. HTS Microstrip Filter

We apply NSM optimization to an HTS quarter-wave parallel coupled-line microstrip filter [9], illustrated in Fig. 8. L_1, L_2, and L_3 are the lengths of the parallel coupled-line sections and S_1, S_2, and S_3 are the gaps between the sections. The width W is the same for all the sections, as well as for the input and output microstrip lines (MSLs), of length L_0. A lanthanum–aluminate substrate with thickness H and dielectric constant ε_r is used.

The specifications are $|S_{21}| \geq 0.95$ in the passband and $|S_{21}| \leq 0.05$ in the stopband, where the stopband includes frequencies below 3.967 GHz and above 4.099 GHz, and the passband lies in the range (4.008 and 4.058 GHz). The design parameters are $\boldsymbol{x}_f = [L_1\ L_2\ L_3\ S_1\ S_2\ S_3]^T$. We take $L_0 = 50$ mil, $H = 20$ mil, $W = 7$ mil, and $\varepsilon_r = 23.425$, loss tangent $= 3 \times 10^{-5}$; the metallization is considered lossless.

Sonnet's ***em***[1] driven by Empipe[2] was employed as the fine model, using a high-resolution grid with a 1 mil $\times$ 1 mil cell size. OSA90/hope[3] built-in linear elements MSL, two-conductor symmetrical coupled microstrip lines (MSCLs), and open circuit (OPEN) connected by circuit theory over the same microstrip substrate definition (MSUB) are taken as the "coarse" model.

The following optimal coarse-model solution is found, as in [10]: $\boldsymbol{x}_c^* = [188.33\ 197.98\ 188.58\ 21.97\ 99.12\ 111.67]^T$ (mils). The coarse- and fine-model responses at the optimal coarse solution are shown in Fig. 9.

The initial $2n+1$ points are chosen by performing sensitivity analysis on the coarse model: a 3% deviation from $\boldsymbol{x}_c^*$ for L_1, L_2, and L_3 is used, while a 20% is used for S_1, S_2, and S_3. The corresponding fine and coarse-model responses at these 13 star-distributed learning points are shown in Fig. 10.

Fig. 11 shows the evolution of the learning errors at the $2n+1$ points as we increase the complexity of the neuromapping

[1]***em***, version 4.0b, Sonnet Software Inc., Liverpool, NY, 1997.

[2]Empipe, version 4.0, Optimization Systems Associates Inc. (now Agilent EEsof EDA), Dundas, ON, Canada, 1997.

[3]OSA90/hope, version 4.0, Optimization Systems Associates Inc. (now Agilent EEsof EDA), Santa Rosa, CA, 1997.

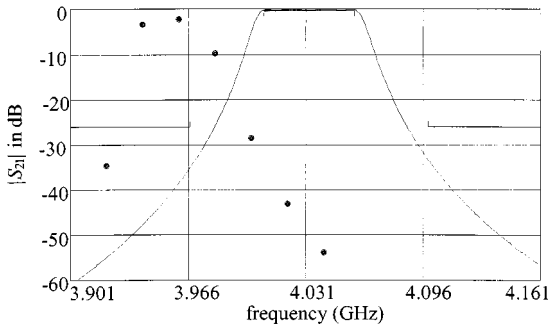

Fig. 9. Coarse- and fine-model responses at the optimal coarse solution: OSA90/hope ($-$) and ***em*** ($\bullet$).

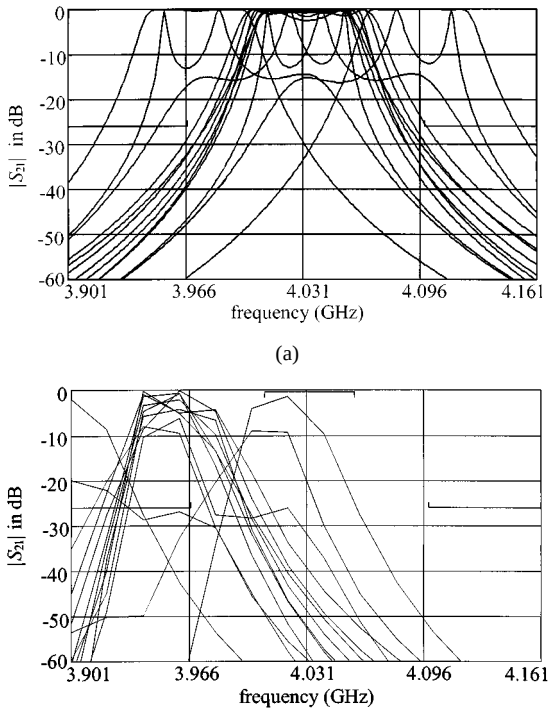

Fig. 10. Coarse- and fine-model responses at the initial $2n + 1$ base points around the optimal coarse solution. (a) OSA90/hope. (b) ***em***.

during the first iteration. All ANNs used in this paper are implemented and trained in OSA90/hope, using Huber optimization, as in [5]. It is seen that mapping the frequency has a dramatic effect on the alignment of the responses, and a simple frequency partial-space mapped neuromapping is needed. The final mapping is implemented with a three-layer perceptron with seven inputs (six design parameters and the frequency), five hidden neurons, and three output neurons (ω, L_1, and S_1).

As indicated in Step 8, we calculate the next point by optimizing the coarse model with the mapping found. The next point predicted is $\boldsymbol{x}_f^{(14)} = [185.37\ 195.01\ 184.24\ 21.04\ 86.36\ 91.39]^T$ (mils), which matches the desired response with excellent accuracy, as seen in Fig. 12. As a final test, both the FPSMN model and fine model are simulated at the NSM solution $\boldsymbol{x}_f^{(14)}$ using a very fine frequency sweep, with a frequency step of 0.005 GHz. The NSM solution satisfies the specifications, as shown in Fig. 13. A detailed illustration of

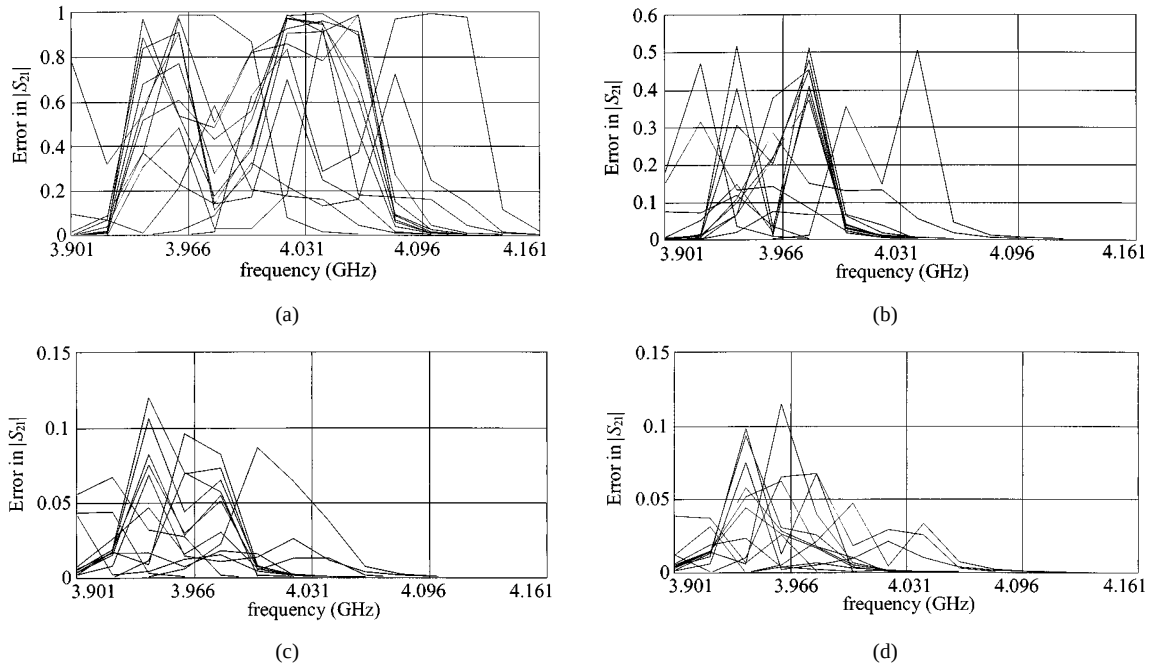

Fig. 11. Learning errors at initial base points. (a) At the starting point. (b) Mapping ω with a 3LP : 7-3-1. (c) Mapping ω and L_1 with a 3LP : 7-4-2. (d) Mapping ω, L_1, and S_1 with a 3LP : 7-5-3.

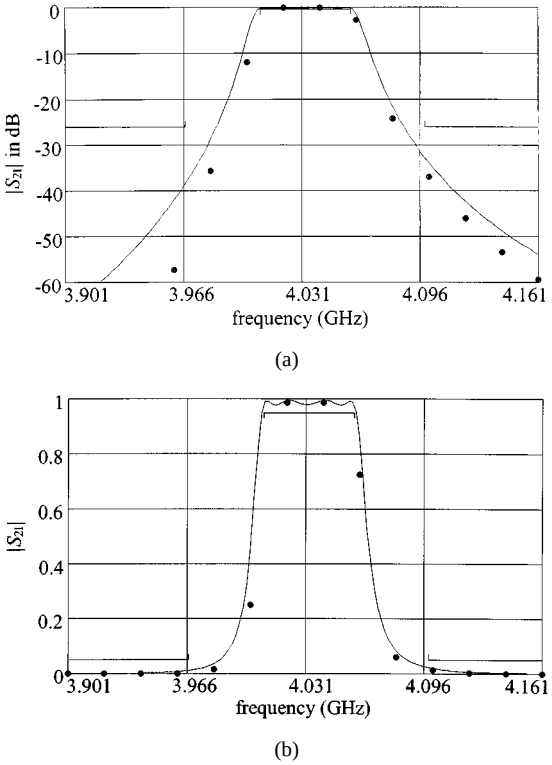

Fig. 12. ***em*** (•) and FPSM 7-5-3 (−) model responses at the next point predicted after the first NSM iteration. (a) $|S_{21}|$ in decibels. (b) $|S_{21}|$.

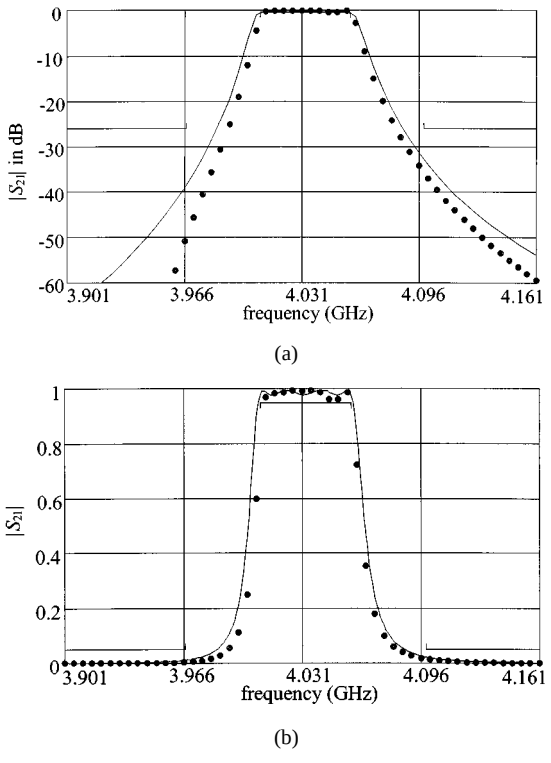

Fig. 13. ***em*** (•) and FPSMN 7-5-3 (−) model responses, using a fine frequency sweep, at the next point predicted after the first NSM iteration. (a) $|S_{21}|$ in decibels. (b) $|S_{21}|$.

the passband using an even finer frequency sweep is shown in Fig. 14. The HTS filter is optimized in only one NSM iteration.

IX. Bandstop Microstrip Filter with Open Stubs

NSM optimization is applied to a bandstop microstrip filter with quarter-wave resonant open stubs, illustrated in Fig. 15. L_1 and L_2 are the open stub lengths and W_1 and W_2 are the corresponding widths. An alumina substrate with thickness $H = 25$ mil, width $W_0 = 25$ mil, and dielectric constant $\varepsilon_r = 9.4$ is used for a 50-Ω feeding line.

The specifications are $|S_{21}| \leq 0.05$ in the stopband and $|S_{21}| \geq 0.9$ in the passband, where the stopband lies between 9.3–10.7 GHz, and the passband includes frequencies below

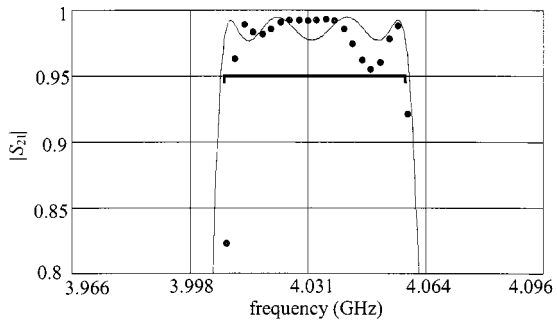

Fig. 14. ***em*** (•) and FPSMN 7-5-3 (−) model responses in the passband, using a fine frequency sweep, at the next point predicted after the first NSM iteration.

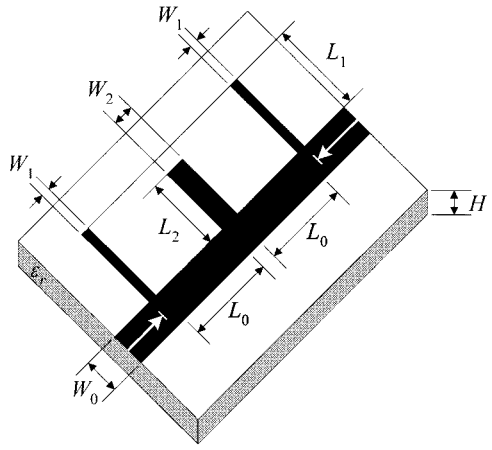

Fig. 15. Bandstop microstrip filter with quarter-wave resonant open stubs.

8 GHz and above 12 GHz. The design parameters are $\boldsymbol{x}_f = [W_1\ W_2\ L_0\ L_1\ L_2]^T$.

Sonnet's ***em*** driven by Empipe was employed as the fine model, using a high-resolution grid with a 1 mil × 1 mil cell size. As a coarse model, we use simple transmission lines for modeling each microstrip section (see Fig. 16) and classical formulas [11] to calculate the characteristic impedance and effective dielectric constant of each transmission line. It is seen that $L_{c2} = L_2 + W_0/2$, $L_{c1} = L_1 + W_0/2$, and $L_{c0} = L_0 + W_1/2 + W_2/2$. We use OSA90/hope built-in transmission-line elements (TRL).

The following optimal coarse-model solution is found for L_0, L_1, and L_2 of quarter-wave lengths at 10 GHz: $\boldsymbol{x}_c^* = [6.00\ 9.01\ 106.45\ 110.15\ 108.81]^T$ (mils). The coarse- and fine-model responses at the optimal coarse solution are shown in Fig. 17.

The initial $2n + 1$ points are chosen by performing sensitivity analysis on the coarse model: a 50% deviation from $\boldsymbol{x}_c^*$ for W_1, W_2, and L_0 is used, while a 15% deviation is used for L_1 and L_2. A simple FM neuromapping (see Fig. 6) with two hidden neurons (3LP : 6-2-1, ω) was used to match the responses at the learning base points. The FM neuromodel and fine-model responses at the optimal coarse solution are shown in Fig. 18. Optimizing the FM neuromodel to satisfy the specifications (Step 8 of the NSM algorithm), the next iterate is $\boldsymbol{x}_f^{(12)} = [6.54\ 16.95\ 91.26\ 113.30\ 120.72]^T$ (mils). The coarse- and fine-model responses at this point are shown in Fig. 19.

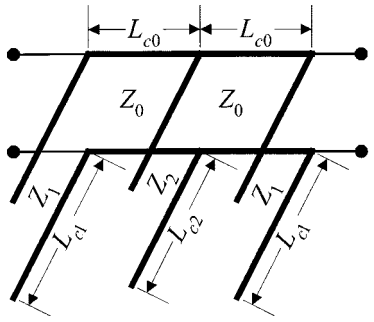

Fig. 16. Coarse model of the bandstop microstrip filter with open stubs.

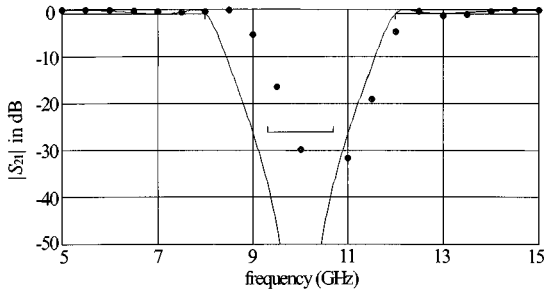

Fig. 17. Coarse- and fine-model responses at the optimal coarse solution: OSA90/hope (−) and ***em*** (•).

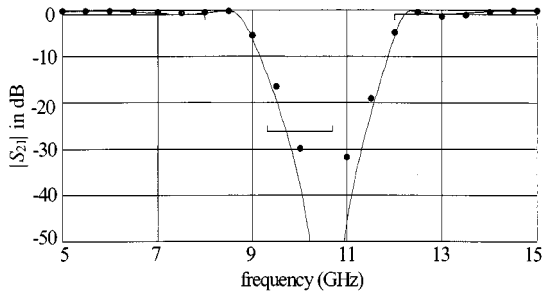

Fig. 18. FM (3LP : 6-2-1, ω) neuromodel (−) and the fine-model (•) responses at the optimal coarse solution.

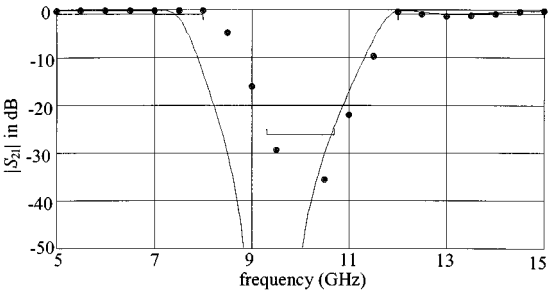

Fig. 19. Coarse- (−) and fine-model (•) responses at the next point predicted by the first NSM iteration.

We performed a second NSM iteration. $\boldsymbol{x}_f^{(12)}$ is included in the learning base points. Now, an FPSM neuromapping with three hidden neurons is needed to match the $2n + 2$ points: only ω and W_2 are mapped (3LP : 6-3-2, ω, W_2). Fig. 20 shows the FPSM neuromodel and fine-model responses at $\boldsymbol{x}_f^{(12)}$. Optimizing the FPSM neuromodel, the next iterate is $\boldsymbol{x}_f^{(13)} = [5.92\ 13.54\ 83.34\ 114.14\ 124.81]^T$ (mils). The

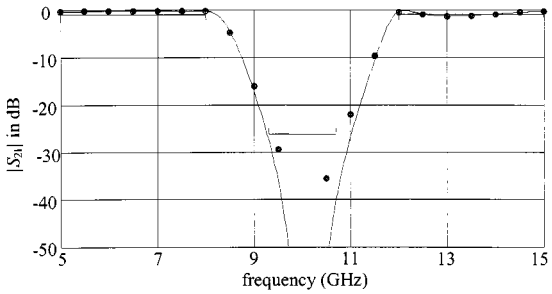

Fig. 20. FPSM (3LP : 6-3-2, ω, W_2) neuromodel ($-$) and the fine-model ($\bullet$) responses at the point predicted by the first NSM iteration.

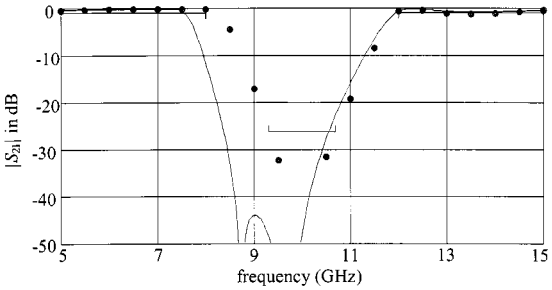

Fig. 21. Coarse- ($-$) and fine-model ($\bullet$) responses at the next point predicted by the second NSM iteration.

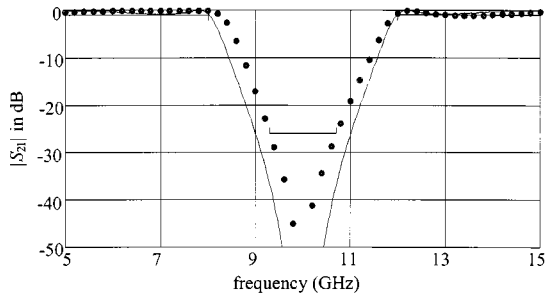

Fig. 22. Fine-model response ($\bullet$) at the next point predicted by the second NSM iteration and optimal coarse response ($-$), using a fine frequency sweep.

coarse- and fine-model responses at $\boldsymbol{x}_f^{(13)}$ are shown in Fig. 21. As final test, using a fine frequency sweep, we show in Fig. 22 the fine-model response at $\boldsymbol{x}_f^{(13)}$ and the optimal coarse response. The bandstop microstrip filter is optimized in two NSM iterations.

X. Conclusion

In this paper, we have presented an innovative algorithm for EM optimization based on SM technology and ANNs. NSM optimization exploits our SM-based neuromodeling techniques to efficiently approximate the mapping from the fine to the coarse input space. NSM does not require parameter extraction to predict the next point. An initial mapping is established by performing upfront fine-model analysis at a reduced number of base points. The coarse-model sensitivities are exploited to select those base points. Huber optimization is used to train simple SM-based neuromodels at each iteration. The SM-based neuromodels are developed without using testing points: their generalization performance is controlled by gradually increasing their complexity starting with a three-layer perceptron with zero hidden neurons. An HTS quarter-wave parallel coupled-line microstrip filter and a bandstop microstrip filter with quarter-wave resonant open stubs illustrate our optimization technique.

Acknowledgment

The authors thank Dr. J. C. Rautio, Sonnet Software Inc., Liverpool, NY, for making ***em*** available.

References

[1] A. H. Zaabab, Q. J. Zhang, and M. S. Nakhla, "A neural network modeling approach to circuit optimization and statistical design," *IEEE Trans. Microwave Theory Tech.*, vol. 43, pp. 1349–1358, June 1995.

[2] P. Burrascano, M. Dionigi, C. Fancelli, and M. Mongiardo, "A neural network model for CAD and optimization of microwave filters," in *IEEE MTT-S Int. Microwave Symp. Dig.*, Baltimore, MD, 1998, pp. 13–16.

[3] P. M. Watson and K. C. Gupta, "Design and optimization of CPW circuits using EM-ANN models for CPW components," *IEEE Trans. Microwave Theory Tech.*, vol. 45, pp. 2515–2523, Dec. 1997.

[4] P. M. Watson, G. L. Creech, and K. C. Gupta, "Knowledge based EM-ANN models for the design of wide bandwidth CPW patch/slot antennas," in *IEEE AP-S Int. Symp. Dig.*, Orlando, FL, July 1999, pp. 2588–2591.

[5] J. W. Bandler, M. A. Ismail, J. E. Rayas-Sánchez, and Q. J. Zhang, "Neuromodeling of microwave circuits exploiting space mapping technology," *IEEE Trans. Microwave Theory Tech.*, vol. 47, pp. 2417–2427, Dec. 1999.

[6] J. W. Bandler, R. M. Biernacki, S. H. Chen, P. A. Grobelny, and R. H. Hemmers, "Space mapping technique for electromagnetic optimization," *IEEE Trans. Microwave Theory Tech.*, vol. 42, pp. 2536–2544, Dec. 1994.

[7] R. M. Biernacki, J. W. Bandler, J. Song, and Q. J. Zhang, "Efficient quadratic approximation for statistical design," *IEEE Trans. Circuit Syst.*, vol. 36, pp. 1449–1454, Nov. 1989.

[8] J. W. Bandler and S. H. Chen, "Circuit optimization: The state of the art," *IEEE Trans. Microwave Theory Tech.*, vol. 36, pp. 424–443, Feb. 1988.

[9] J. W. Bandler, R. M. Biernacki, S. H. Chen, W. J. Getsinger, P. A. Grobelny, C. Moskowitz, and S. H. Talisa, "Electromagnetic design of high-temperature superconducting microwave filters," *Int. J. Microwave Millimeter-Wave Computer-Aided Eng.*, vol. 5, pp. 331–343, 1995.

[10] M. H. Bakr, J. W. Bandler, R. M. Biernacki, S. H. Chen, and K. Madsen, "A trust region aggressive space mapping algorithm for EM optimization," *IEEE Trans. Microwave Theory Tech.*, vol. 46, pp. 2412–2425, Dec. 1998.

[11] M. Pozar, *Microwave Engineering*. New York: Wiley, 1998, p. 162.

Mohamed H. Bakr (S'98) was born in November 7, 1969. He received the B.Sc. degree (with distinction) in electronics and communications engineering and the M.Sc. degree in engineering mathematics from Cairo University, Cairo, Egypt, in 1992 and 1996, respectively, and the Ph.D. degree in electrical and computer engineering from McMaster University, Hamilton, ON, Canada, in 2000.

In October 1992, he joined the Department of Engineering Mathematics and Physics, Faculty of Engineering, Cairo University. In September 1996, he joined the Department of Electrical and Computer Engineering, McMaster University, where his research is carried out in the Simulation Optimization Systems Research Laboratory. He held the position of a student intern at Optimization Systems Associates Inc. from July 1997 to June 1998. He is currently a Post-Doctoral Fellow in the Department of Electrical and Computer Engineering, McMaster University. He is interested in optimization methods, computer-aided design, and modeling of microwave circuits and in neural-networks applications.

Mr. Bakr has held the Ontario Graduate Scholarship (OGS) for two consecutive years. He was also awarded a Natural Sciences and Engineering Research Council of Canada (NSERC) Post-Doctoral Fellowship in April 2000.

John W. Bandler (S'66–M'66–SM'74–F'78) was born in Jerusalem, on November 9, 1941. He studied at the Imperial College of Science and Technology, London, U.K., from 1960 to 1966. He received the B.Sc. (Eng.), Ph.D., and D.Sc. (Eng.) degrees from the University of London, London, U.K., in 1963, 1967, and 1976, respectively.

In 1966, he joined Mullard Research Laboratories, Redhill, Surrey, U.K. From 1967 to 1969, he was a Post-Doctorate Fellow and Sessional Lecturer at the University of Manitoba, Winnipeg, MB, Canada. In 1969, he joined McMaster University, Hamilton, ON, Canada, where he has served as Chairman of the Department of Electrical Engineering and Dean of the Faculty of Engineering. He is currently a Professor Emeritus in Electrical and Computer Engineering, and directs research in the Simulation Optimization Systems Research Laboratory. He is a member of the Micronet Network of Centres of Excellence. He was President of Optimization Systems Associates Inc. (OSA), which he founded in 1983, until November 20, 1997, the date of acquisition of OSA by Hewlett-Packard Company (HP). OSA implemented a first-generation yield-driven microwave computer-aided design (CAD) capability for Raytheon in 1985, followed by further innovations in linear and nonlinear microwave CAD technology for the Raytheon/Texas Instruments Incorporated Joint Venture MIMIC Program. OSA introduced the computer-aided engineering (CAE) systems RoMPE in 1988, HarPE in 1989, OSA90 and OSA90/hope in 1991, Empipe in 1992, and Empipe3D and EmpipeExpress in 1996. OSA created the product ***empath*** in 1996, which was marketed by Sonnet Software Inc., Liverpool, NY. He is President of the Bandler Corporation, Dundas, ON, Canada, which he founded in 1997. He has authored or co–authored over 320 papers from 1965 to 2000. He contributed to *Modern Filter Theory and Design* (New York: Wiley, 1973) and to *Analog Methods for Computer-aided Analysis and Diagnosis* (New York: Marcel Dekker, 1988). Four of his papers have been reprinted in *Computer-Aided Filter Design* (New York: IEEE Press, 1973), one in each of *Microwave Integrated Circuits* (Norwood, MA: Artech House, 1975), *Low-Noise Microwave Transistors and Amplifiers* (New York: IEEE Press, 1981), *Microwave Integrated Circuits, 2nd ed.* (Norwood, MA: Artech House, 1985), *Statistical Design of Integrated Circuits* (New York: IEEE Press, 1987), and *Analog Fault Diagnosis* (New York: IEEE Press, 1987). He joined the Editorial Boards of the *International Journal of Numerical Modeling* in 1987, the *International Journal of Microwave and Millimeterwave Computer-Aided Engineering* in 1989, and *Optimization and Engineering* in 1998. He was guest editor of the *International Journal of Microwave and Millimeter-Wave Computer-Aided Engineering* "Special Issue on Optimization-Oriented Microwave CAD" (1997).

Dr. Bandler is a Fellow of the Royal Society of Canada, a Fellow of the Institution of Electrical Engineers (IEE), U.K., a Fellow of the Engineering Institute of Canada, a member of the Association of Professional Engineers of the Province of Ontario (Canada), and a member of the Massachusetts Institute of Technology (MIT) Electromagnetics Academy. He was an associate editor of the IEEE TRANSACTIONS ON MICROWAVE THEORY AND TECHNIQUES (1969–1974), and has continued serving as a member of the Editorial Board. He was guest editor of the Special Issue on "Computer-Oriented Microwave Practices" of the IEEE TRANSACTIONS ON MICROWAVE THEORY AND TECHNIQUES (1974), guest co-editor of the Special Issue on "Process-Oriented Microwave CAD and Modeling" of the IEEE TRANSACTIONS ON MICROWAVE THEORY AND TECHNIQUES (1992), and guest editor of the Special Issue on "Automated Circuit Design Using Electromagnetic Simulators" of the TRANSACTIONS ON MICROWAVE THEORY AND TECHNIQUES (1997). He is currently co-chair of the MTT-1 Technical Committee on Computer-Aided Design. He was the recipient of the 1994 Automatic Radio Frequency Techniques Group (ARFTG) Automated Measurements Career Award.

Mostafa A. Ismail (S'98) was born in Cairo, Egypt, on May 21, 1968. He received the B.Sc. degree in electronics and communications engineering and the Masters degree in engineering mathematics from Cairo University, Cairo, Egypt, in 1991 and 1995, respectively, and is currently working toward the Ph.D. degree at McMaster University, Hamilton, ON, Canada.

In October 1991, he joined the Department of Engineering Mathematics and Physics, Faculty of Engineering, Cairo University. In September 1997, he joined the Department of Electrical and Computer Engineering, McMaster University, where his research is carried out in the Simulation Optimization Systems Research Laboratory. His research interests are computer-aided design and modeling of microwave circuits.

Mr. Ismail was the recipient of a one-year Nortel Networks Ontario Graduate Scholarship in Science and Technology in 2000.

José Ernesto Rayas-Sánchez (S'88–M'89–SM'95) was born in Guadalajara, Jalisco, Mexico, on December 27, 1961. He received the B.Sc. degree in electronics engineering from the Instituto Tecnológico y de Estudios Superiores de Occidente (ITESO), Guadalajara, Mexico, in 1984, the Masters degree in electrical engineering at the Instituto Tecnológico y de Estudios Superiores de Monterrey (ITESM), Monterrey, Mexico, in 1989, and is currently working toward the Ph.D. degree in electrical engineering at McMaster University, Hamilton, ON, Canada.

From 1989 to 1997, he was a Full-Time Professor in the Electrical and Computer Engineering Department, ITESO. He joined the Simulation Optimization Systems Research Laboratory, McMaster University, in 1997. His research focuses on the development of novel methods and techniques for computer-aided modeling, design, and optimization of analog wireless electronic circuits and devices exploiting SM and ANNs.

Mr. Rayas-Sánchez was the recipient of a 1997–2000 Consejo Nacional de Ciencia y Tecnología (CONACYT) Scholarship presented by the Mexican Government, as well as a 2000–2001 Ontario Graduate Scholarship presented by the Ministry of Training for Colleges and Universities in Ontario.

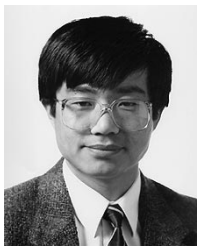

Qi-Jun Zhang (M'87-SM'95) received the B.Eng. degree from East China Engineering Institute, Nanjing, China, in 1982, and the Ph.D. degree in electrical engineering from McMaster University, Hamilton, ON, Canada, in 1987.

In 1982 and 1983, he was with the System Engineering Institute, Tianjin University, Tianjin, China. From 1988 to 1990, he was with Optimization Systems Associates Inc. (OSA), Dundas, ON, Canada, where he developed advanced microwave optimization software. In 1990, he joined the Department of Electronics, Carleton University, Ottawa, ON, Canada, where he is currently a Professor. His research interests are neural-network and optimization methods for high-speed/high-frequency circuit design. He has authored *Neural Networks for RF and Microwave Design* (Norwood, MA: Artech House, 2000), co-edited *Modeling and Simulation of High-Speed VLSI Interconnects* (Norwell, MA: Kluwer), and contributed to *Analog Methods for Computer-Aided Analysis and Diagnosis* (New York: Marcel Dekker, 1988). He was a Guest Co-Editor for the Special Issue on "High-Speed VLSI Interconnects" for the *International Journal of Analog Integrated Circuits and Signal Processing* (Norwell, MA: Kluwer, 1994), a Guest Editor for the first Special Issues on "Applications of ANN to RF and Microwave Design" for the *International Journal of RF and Microwave Computer-Aided Engineering* (New York: Wiley, 1999), and a Guest Editor for the second Special Issues on "Applications of ANN to RF and Microwave Design" for the *International Journal of RF and Microwave CAE* (New York: Wiley, to be published in 2001).

Dr. Zhang is a member of the Association of Professional Engineers Ontario.